Al-Zn Alloy Formation by Aluminium Underpotential Deposition from AlCl₃+NaCl Melts on Zinc Substrate

Niko Jovićević[1], Vesna S. Cvetković[2], Željko J. Kamberović[1], Jovan N. Jovićević[2,]*

[1] Faculty of Technology and Metallurgy, University of Belgrade, Karnegijeva 4, 11120 Beograd, Serbia
[2] Faculty of Sciences and Mathematics, University of Priština, I.L.Ribara 29, 38220 K. Mitrovica. Serbia
[*]E-mail: matori47@hotmail.com

Aluminium was incorporated into polycrystalline zinc electrode surface by underpotential deposition from equimolar AlCl₃+NaCl melt at 473, 523 and 573 K. The process was studied by linear sweep voltammetry and potentiostatic deposition/galvanostatic striping. The deposits were characterised by glancing incidence X-ray diffraction (GIXRD), Auger (AES) and electron probe micro-analyzer (EPMA). The electrochemical measurements showed evidence of Zn − Al alloys being formed. The constant-potential regions measured during the low-current striping correspond to the coexistence of two pairs of metastable intermetallic phases. However, the observed alloys could not be identified. The growth kinetics of the compounds is described.

1. INTRODUCTION

One of the ways to obtain metal and its alloys is electrochemical deposition [1, 2], but neither aluminium nor its alloys can be electrodeposited from aqueous solutions because hydrogen starts evolving before aluminium is plated. The chloroaluminate melts [3, 4] containing inorganic [3, 5−7] or organic [3, 8, 9−11] chloride salts combined with anhydrous aluminium chloride have been successfully used for electrodeposition of different metals and theirs alloys onto different substrates [3, 8, 12].

The studies of metal deposition from solutions [13−16] revealed that a metal, electrodeposited onto another metal cathode at potentials more positive than the reversible potential of the depositing metal (underpotential deposition − UPD) into which it can diffuse at room temperature, can make a

surface alloy with the substrate [17−19]. Soon it was found to be true for underpotential deposition of aluminium on some metals from inorganic [3, 20−25] and organic melts also [3, 26, 27], too.

UPD of metals from solutions [17, 18, 28, 29] and formation of alloys by UPD of aluminium from inorganic melts onto surface of different metals [6, 21−26] has been a subject of our work for more than twenty years. Aluminium UPD from $AlCl_3$+NaCl melt on several metal electrodes [6] inducing surface alloy formation lead to more elaborate studies of aluminium UPD on Au [21], Ag [22], Cu [23] and Fe [24]. It was found that at temperatures from 473 K to 573 K, four Au−Al, two Ag−Al, four or more Cu−Al and three Fe−Al alloys were formed by diffusion of underpotentially deposited aluminium into gold, silver, copper and iron substrate, respectively. Similar results were obtained by others on gold [27, 30] and copper [3, 30] from organic melts.

There are very few records of Al–Zn alloy formation by overpotential codeposition [12, 8, 31–34] of Zn and Al from organic melts – ionic liquids. However, in literature there are no detailed studies of aluminium UPD on zinc from inorganic melts, although according to the theory [13, 14] it might be expected.

In the present study, the UPD of aluminium on policrystalline substrate of zinc from $AlCl_3$+NaCl equimolar melts was investigated by electrochemical techniques and surface analysis. The data on the influence of temperature and deposition time were correlated with the analysis results to produce data describing possible formation of intermetallic compounds.

2. EXPERIMENTAL

2.1. Electrochemical experiments

All electrochemical experiments were carried out in an electrochemical cell placed in a furnace and designed for work with melts under a purified argon atmosphere, described in details elsewere [21–24].

Aluminium wire 3mm in diameter (99,999% pure, Alfa Products, Thiokol/Ventron division, USA) was used as a reference electrode in a Luggin capillary whose tip was placed close to the working electrode. An aluminium plate (99,999% pure, Alfa Products, Thiokol/Ventron division, USA) was used as a counter electrode. Two types of sizes of working electrode were used. The one for electrochemical experiments consisted of 1mm diameter 99,99% pure zinc wire pressed into a glass tube of slightly larger diameter such that only $1cm^2$ area of the metal wire was exposed to the melt. The other was $2 cm^2$ 99,99% pure zinc plate working electrode for surface/sub-surface analysis. It was clipped (above the melt surface) onto a conductive wire pressed into a glass tube allowing the electrode surface area of $1 cm^2$ to be exposed to contact with melt.

The aluminium reference and counter electrodes were first mechanically polished on emery papers and then on polishing cloths ("Beuhler Ltd.") impregnated with alumina ("Banner Scientific Ltd."). After mechanical polishing, the electrodes were etched in solutions of 50 vol.% HF + 15 vol.% H_2O and NH_4OH (conc. 96%) + 5 vol.% H_2O_2 prior to each experiment.

Zinc working electrodes for electrochemical experiments were mechanically polished and before introduction into the process each electrode was subsequently chemically polished in the acid mixture (300 g L^{-1} chromic acid + 30 g L^{-1} sodium sulphate), stirred for 15−20 seconds and then rinsed with plenty of tap water. When yellowish film appeared on the zinc surface the electrode was dipped into sulphuric acid solution (75 g L^{-1} of H$_2$SO$_4$) until the film disappeared. The procedure was repeated two to three times and eventually the electrode was rinsed with triply distilled water. The working electrodes–samples for surface/sub-surface analysis were prepared in the same way. Examination of the electrode surface under the optical microscope and with X-ray emission spectroscopy revealed no contaminating elements.

In order to remove bonded water the sodium chloride was mechanically reduced to fine powder, dried in a furnace at 773 K for five hours and kept in vacuum at 393 K until use. No drying procedure was applied to aluminium (III) chloride; instead, fresh, sealed bottle of anhydrous AlCl$_3$ (99,99 % pure AlCl$_3$, "Aldrich Chemical Company, Inc.") was used for each experiment. The procedure of melting the AlCl$_3$+NaCl mixture consisted of heating NaCl on top of AlCl$_3$ at 523 K (in an inert atmosphere), allowing the AlCl$_3$ to sublime forming a homogeneous AlCl$_3$+NaCl melt by the reaction with NaCl. The melt was subjected to preelectrolysis for 10 hours with constant current density $i = 1,5·10^{-2}$A cm^{-2} between two electrodes-aluminium plates (99,999 % Al) of 20 cm^2 each at 493-523 K. The surface of the aluminium plates was prepared in the same way as the surface of the reference electrode. After the preelectrolysis, linear sweep voltammogram obtained on vitreous carbon showed only double layer charging and discharging between 0,005 – 1,85V vs. Al.

Two electrochemical techniques were used: linear sweep voltammetry (LSV) and potentiostatic UPD followed by galvanostatic stripping. Two different procedures of LSV were carried out one after the other:

a)   first the potential range was scanned from a potential 0,050 – 0,060 V negative to the open circuit potential of the zinc electrode (0,220 – 0,250 V measured against the aluminium reference electrode) to a potential 0,030 – 0,040 V positive to the reversible aluminium potential, followed by the return scan. The sweep rate was 0,010 V s^{-1};

b)   then the same potential range was scanned except that the scan was interrupted when the potential reached 0,030 – 0,040 V positive to the reversible aluminium potential; and this potential was held for $\tau_d = 1, 3, 6, 9$ and 15 minutes before starting the return scan. The sweep rate was as in a).

The procedure for the potentiostatic UPD followed by galvanostatic stripping was as follows:

a)   the specimen was held at 0,050 – 0,060 V negative to the open circuit potential of zinc (0,220 – 0,250 V vs. Al), to strip any aluminium already deposited. Then the potential was stepped to the 0,030 – 0,040 V from the reversible potential of aluminium;

b)   this potential ($E_d = 0,030 – 0,040$ V vs. Al) was maintained for $\tau_d = 1, 3, 6, 9$ min after which the potential was switched out of circuit to open the electrode circuit. The electrode potential was then recorded by an XY recorder as a function of time, whilst a small current ($\cong 0,02$ mA cm^{-2}) slowly stripped the aluminium from the surface of zinc specimen. If the stripping current was interrupted for a few seconds, the measured potential did not detectably change. This showed that the activation overpotential caused by the stripping current was negligible and the potentials measured can be considered "open circuit" potentials.

All electrochemical measurements were carried out using a potentiostat (PAR -M273A) and an *X-Y-t* recorder (Hewlet Packard M7040A). The temperature of the melt was monitored by a chromel-alumel thermocouple with an accuracy of 1^oC.

2.2. *Surface/sub-surface analysis*

Glancing incidence X-ray diffraction (GIXRD) and electron microprobe analysis (EPMA) of polished cross-sections were used as techniques for surface/sub-surface analysis. These techniques were applied comparatively to blank probes polished mechanically and chemically and samples after electrochemical UPD. Sample preparation for the surface/sub-surface analysis was as follows: aluminium was electrodeposited from the equimolar $AlCl_3$+NaCl melt at constant underpotential ($E_d =$ 0,030 – 0,040 V vs. Al) for different periods of time (τ_d = 1, 2 and 4 h) at three different temperatures (473, 523 and 573 K). Deposition was started 5 min after insertion of the working electrode in order to allow thermal equilibrium. The working electrode was then removed from the melt whilst still under polarisation, then washed repeatedly under distilled water, air dried and stored in a desiccator until use.

The crystallographic structure present near the surface of these specimens was determined using glancing angle X-ray diffraction at an incident angle of 1° to the surface. A multipurpose glancing angle X-ray spectrometer using a standard X-ray tube and germanium solid state detector was used. The spectrometer was controlled by an IBM-PC-T computer with Superior electric microstepping motors powering various goniometer motions. The detector pulses were timed and counted using a Tecmar Labmaster interface.

To prepare cross-sections for EPMA examination, samples which had been used as working electrodes were first cut into smaller plates, typically 1/3 of the original size. These were supported vertically in clips and covered with conductive plastic powder. The sample in powder was then pressed into a disc (2,5cm diameter and 1cm height) and the remaining visible edge of the sample polished to 0,1 mm, EPMA was carried out using a CAMEBAX-R electron microprobe.

Auger electron spectroscopy (AES), (Perkin-Elmer 560 ESCA/SAM equipped with a cylindrical mirror analyser), was used to obtain the composition−depth profile of the specimen under the surface.

3. RESULTS AND DISCUSSION

Examples of the linear sweep voltammograms for aluminium underpotential deposition on zinc electrodes at different deposition times (τ_d) and at various temperatures (*T*) is shown in Fig. 1.
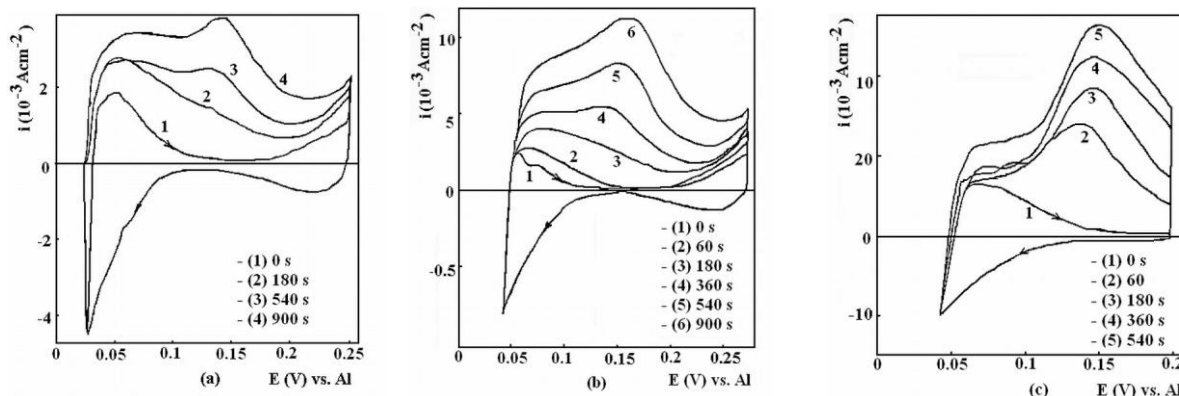
Figure 1. Linear sweep voltammograms of aluminium dissolution from zinc electrode obtained with a sweep rate 10 mVs^{-1} at: a) 473 K; b) 523 K and c) 573 K.

The potential values E (V vs. Al) and the corresponding current densities i (10^{-3} Acm^{-2}) for the dissolution peaks observed in the anodic parts of the voltammograms as a function of the deposition time τ_d, and temperature T, are summarized in Table 1.

Table 1. Peak potentials E (V vs. Al) and the corresponding anodic current densities i (10^{-3} Acm^{-2}) observed in the anodic part of linear sweep voltammograms on zinc electrodes as a function of deposition time τ_d (s) and temperature T (K).

τ_d(s)	0		60		180		360		540		900	
T(K)	E	i	E	i	E	i	E	i	E	i	E	I
473	0,07	0,19	-	-	0,07	2,77			0,07	2,77	0,07	3,20
	-	-	-	-	-	-		-	0,15	2,30	0,15	3,80
523	0,05	2,50	0,06	2,60	0,08	4,70	0,08	5,00	0,08	6,67	0,08	8,33
	-	-	-	-	-	-	0,150	6,11	0,160	8,61	0,155	11,66
573	0,07	5,70	0,07	6,00	0,075	7,50	0,075	8,00	0,07	11,00		
	-	-	0,15	12,9	0,150	17,00	0,150	22,00	0,15	25,00		

The total anodic dissolution charge $Q_{Al,max}$ and calculated mass of aluminium deposited on zinc electrodes, as a function of the deposition time and temperature, are listed in Table 2. $Q_{Al,max}$ values were obtained by integration of the linear sweep voltammograms to give the surface area bounded by the anodic current and the horizontal axis. The values E, i_p and $Q_{Al,max}$ presented in Table 1 and Table 2 are average values obtained from five or more measurements. The mass of aluminium deposited was calculated from Faraday's law.

Table 2. Total anodic dissolution charges (mC cm^{-2}) and mass calculated of Al deposited (10^{-6}g cm^{-2}) as a function of deposition time τ_d (s) and temperature T (K) for zinc electrodes.

T(K)	τ_d (s)	0	60	180	360	540
473	Total anodic charge	14,5	25,2	32,4	38,9	40,3
	Mass of Al deposited	1,36	2,37	3,05	3,66	3,79
523	Total anodic charge	16,2	41,1	53,8	72,6	91,1
	Mass of Al deposited	1,52	3,86	5,06	6,82	8,56
573	Total anodic charge	37,2	118,6	168,1	234,9	250,9
	Mass of Al deposited	3,5	11,5	15,8	22,08	23,59

Representatives of the potential/time diagrams of aluminium dissolution from zinc electrodes, obtained by low-current galvanostatic stripping („open circuit measurements") folowing UPD of various times and different temperatures, are given in Fig. 2. and Table 3. which summarize the average potential values at the observed plateaux for five or more measurements.
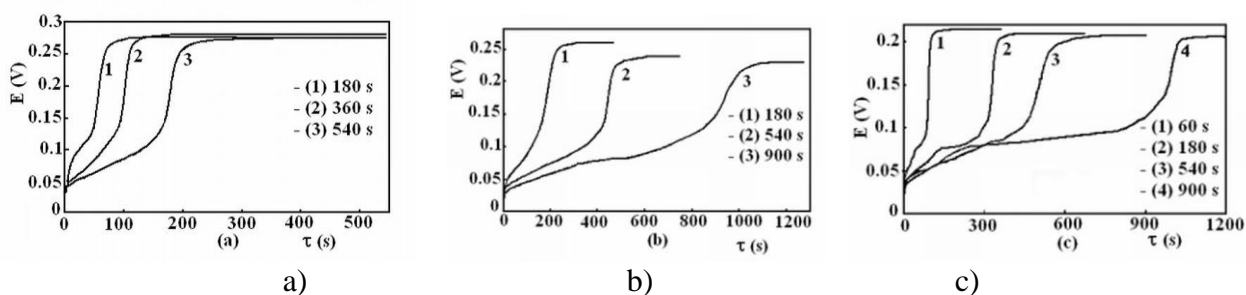

a)   b)   c)

Figure 2. „Open circuit" graphs of aluminium dissolution from zinc electrodes at: a) 473 K; b) 523 K; c) 573 K.

Table 3. Inflection points and the corresponding values E (V vs. Al) obtained in „open circuit" measurments of aluminium deposited on zinc at different times τ_d (s) and various temperatures T (K).

T(K)	473			523			573		
τ_d(s)	180	360	540	180	540	900	180	360	540
Inflection point potential (V vs. Al)	0,044	0,044	0,044	0,050	0,045	0,040	0,042	0,041	0,037
	0,085	0,065	0,050	0,060	0,066	0,078	0,076	0,080	0,074

Examples of the diffraction patterns taken of the zinc samples after aluminium underpotential deposition as a function of temperature and deposition time are given in Fig. 3. The 2θ values that

could be attributed neither to Zn [35–37] nor to Al [38] and have not been recognized by Al-Zn phase diagram [49,50] are marked by question marks on the figures and listed in Table 4. The peak corresponding to 2θ value of 43,9° in Fig. 3a) (marked as Al) could be regarded as somewhat moved 2θ value of 44,72° reported as corresponding to the diffraction of Al (200) layer [35].
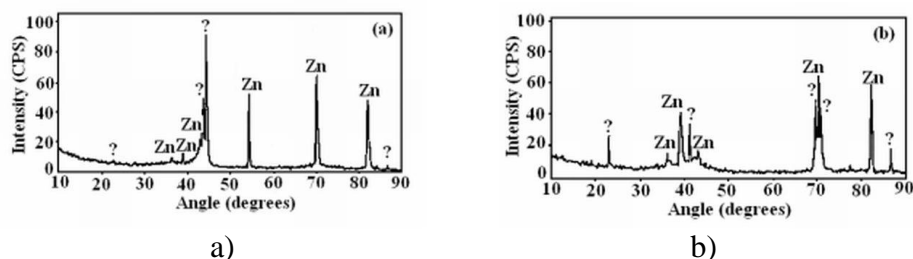

a)   b)

Figure 3. Diffraction patterns of zinc samples after aluminium underpotential deposition at 523 K for: a) one and b) two hours.

Table 4. 2θ values (degrees) for unattributed X-Ray diffraction peaks from the diffraction patterns of zinc samples after aluminium deposition of one and two hours at 523 K.

T(K)	τ_d (hour)	2θ
	1	23,0°, 43,9°, 86,6°
523	2	23,0°, 42,2°, 69,8°, 71,1°, 86,86°

Figure 4. shows characteristic EPMA spectra taken within 1 μm of the edge of the cross-sectioned zinc samples after aluminium uderpotential deposition at 523 K for different times. No quantitative analysis was possible because the thickness of the detected layer was less than the lateral resolution of the EPMA analysis. Therefore, these diagrams present only a very tentative qualitative indication of posible Al presence in the surface of the zinc samples.
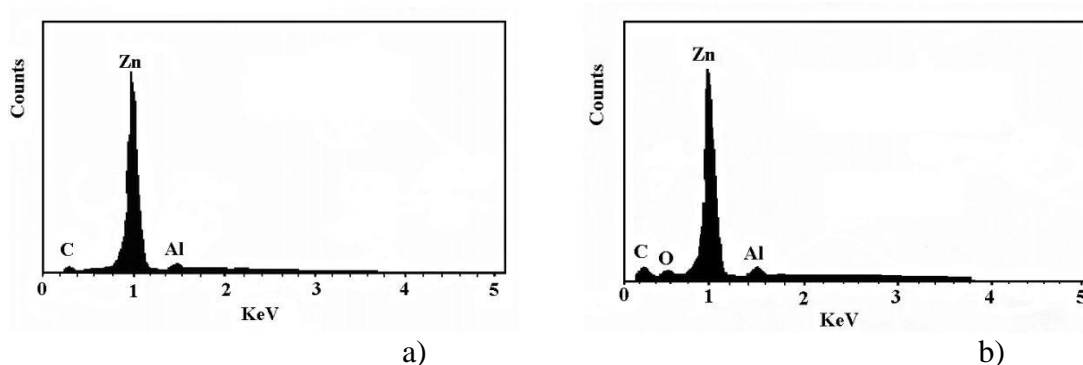

a)   b)

Figure 4. Characteristic EPMA spectra of zinc samples after: a) one, and b) two hours of aluminium underpotential deposition at 523 K.

3.1. Linear sweep voltammograms: influence of deposition time and temperature

The reversible potential of the zinc substrate was more positive than the reversible potential of aluminium in the same system which allowed the phenomenon of aluminium underpotential deposition (UPD) on zinc to be studied.

In general, the total recorded charges bounded by the cathodic and anodic currents were similar (within ± 5% difference) and symmetrical to the zero current axes, but the fine structure of the cathodic current peaks of linear sweep voltammograms was less pronounced than the anodic one. The anodic current peaks, however, were more readily defined, particularly in the case of a prolonged underpotential deposition.

Instead of recording the potential at the beginning of corresponding anodic and cathodic peaks the current peak potential values were measured between peak valleys values because cathodic peak separation was not as well pronounced as in the case of single crystal substrates [15–17] which prevented exact cathodic to anodic peak attribution and because anodic current peaks were well merged thus preventing exact allocation of the peak starting potential.

The charge calculated for cathodic and anodic parts of the linear sweep voltammograms obtained, were significantly different from the charge needed for the deposition of the closest packed aluminium monolayer (Al atomic radius being $1{,}18 \cdot 10^{-10}$ m) we calculated to be 1,17 mC cm^{-2}.

When the chosen cathodic end potentials, E_d, were maintained for longer times during linear sweep experiments, the cathodic current increase was not observed. This would suggest that the aluminium underpotential deposition after at least one aluminium monolayer completion proceeds at the rate necessary to compensate for the amount lacking of one aluminium monolayer which entered solid state intermetallic reaction with the substrate - zinc. This dynamic quasi-equilibrium would seem to be maintained as long as intermetallic solid state reaction proceeded by diffusion of aluminium into the substrate. Different anodic dissolution peaks would, then, reflect different intermetallic compounds formed during previous aluminium deposition, having naturally different dissolution potentials [3,21–24] (Fig. 1.).
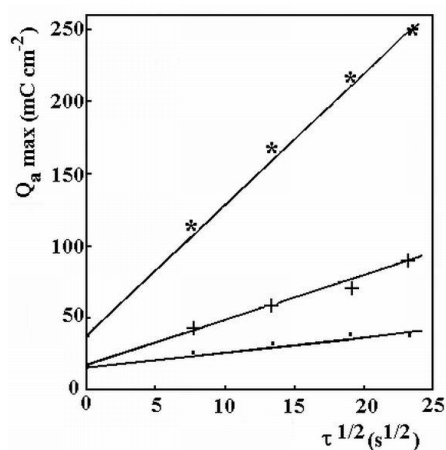

Figure 5. Charge of aluminium dissolution $Q_{Al,(max)}$, as a function of $\tau^{1/2}$, at (▪) 473 K, (+) 523 K and (*) 573 K for zinc electrode.

When the holding (the deposition time, τ_d) of the zinc electrode at the cathodic end potential, E_d, was increased, two characteristics of the anodic current peaks could be observed:

- anodic peak current values, i_p, increased with the cathodic end potential holding time τ_d;

and the integrated charge under each of the anodic peaks (as well as the total anodic charge, $Q_{Al,max}$) increased proportionally to the square root of the cathodic end potential holding time $\tau_d^{1/2}$ (see Table 1, Table 2 and Fig.5.).

It should be noted that the increase in working temperature of the system, all other conditions being kept the same, led to the increase of the charge under both cathodic and anodic peaks. Also, as it can be seen in Table 1, the anodic peak current values increased with increasing working temperature.

LSV data obtained strongly suggest that, under the given conditions, underpotentially deposited aluminium diffuses into zinc substrate forming surface alloys [17−19, 21−24].

3.2. Low-current galvanostatic stripping

To obtain the dissolution characteristics of the underpotentially deposited aluminium onto and into the zinc substrate, the potential pulse with amplitude cathodically exceeding the potentials characteristic for the appearance of anodic peaks (E_d = 0,030 − 0,040 V vs. Al) was followed by a quasi open circuit measurement of the electrode potential over time. The small constant dissolution current applied in the "open circuit" measurements resulted in the potential-time curves exhibiting plateaux brought about by dissolution material being able to sustain an equilibrium potential (or corrosion potential) with $AlCl_4^-$ in the melt, Fig. 2 [14, 21−24, 42]. The number of plateaux (Table 3) can be seen to agree with the number of anodic peaks obtained during the linear sweep measurements (Table 1). The potentials of the two plateaux in Fig. 2. correspond reasonably well to the potentials of the anodic current peaks in the LSV's. The existence of peaks in the linear sweep voltammograms indicate that these potentials are indeed reversible potentials (irreversible potential contributions such as activation overpotentials or diffusion overpotentials would increase monotonically with overpotential and not result in peaks).

In fact, when the cathodic pulse amplitude applied was more negative than the potential of the most anodic peak observed on the linear sweep voltammogram, the plateau at the potential similar to the linear sweep voltammogram peak potential was recorded in the potential-time curve of the "open circuit" measurement. When potential pulse amplitude exceeded both linear sweep voltammogram peak potentials, the potential-time curves of the "open circuit" showed two at the potentials very close to the voltammogram peak potentials. This allowed the charge belonging to each of the plateaux (aluminium-zinc alloy) produced during potential step to be calculated on the basis of the time it took to be dissolved (dissolution current density being constant at 0,02 mAcm^{-2}). The charges of cathodic deposition processes corresponded well to the anodic dissolution charges (within ±5%) calculated as the multiple of dissolution current density and the time elapsed for the dissolution. Comparison of the charges obtained this way agreed very well (within ±5%) with the charges under the anodic peaks limited by the same potential range in the LSV voltammetry.

Prolonged potentiostatic underpotential deposition brought about a proportional increase in the "open circuit" dissolution time, but this had little effect on the potentials of the plateaux. An increase in the working temperature, however, increased the amount of aluminium deposited and dissolved. This is again consistent with the previously described linear sweep voltammetry results [21−24].

The "open circuit" measurements, and particularly:

a.-   the existence of the reversible (or corrosion) potential (two of them apart from reversible potential of zinc substrate),

b.-   the temperature dependence of these potentials,

c.-   very similar behaviour of these potentials and the reversible aluminium potential,

gave strong support to the assumptions already made earlier that intermetallic compounds are formed between zinc substrate and underpotentially deposited aluminium.

3.3. Alloy formation

Both, the linear sweep voltammograms of aluminium deposition/dissolution (Fig. 1) and low-current galvanostatic stripping measurements (Fig. 2), clearly show that some interaction between the substrate (zinc) and aluminium from the melt occurs at a potential positive to the potential of the aluminium reference electrode. Absence of an increase in the cathodic current during holding at the cathodic-end potential suggests no nucleation barrier for alloy formation and indicates that a dynamic quasi-equilibrium is maintained at the surface of the zinc electrode by diffusion of the aluminium into the zinc substrate. The aluminium–zinc phase diagram [36–41] for the temperatures applied shows possibility of numerous intermetallic compounds being formed. Therefore, two anodic dissolution peaks recorded in voltammograms could be ascribed to the aluminium dissolution from different intermetallic compounds, having naturally different dissolution potentials. The GIXRD and EPMA analysis, Fig. 3 and 4, were in accordance with such a proposition.

With increasing melt temperature alloying of zinc with aluminium in the underpotential region becomes more pronounced, indicating that diffusion of aluminium in the solid state becomes faster at higher temperatures, Fig. 5.

The potential-time graphs obtained during low-current galvanostatic stripping (″open circuit″ measurements) provide estimates of the reversible aluminium potential corresponding to the phases on the zinc surface, as well as for the reversible potential of zinc (E_{rev} V vs. Al). This is possible because the low-current gave rise to the negligible activation overpotential; the measured potential showed no immediate change when the current was interrupted. Applying the Nernst equation [42] to the potentials reported in Table 3 gives information on the partial molar Gibbs energy of aluminium existing on the surface of zinc at various times. This is constant when pairs of phases co-exist at the substrate surface, except for E_{rev} (V vs. Al) where flattening of the top end of the curve. Fig. 2, merely reflects the fact that aluminium becomes exhausted at the surface after some time. It seems obvious that the number of plateaux observed in Fig. 2, and from the data in Tables 3 and 4, equals the number of two two-phase regions. It was impossible to define what those two intermetallic phases were. It should not be surprising, because at temperatures bellow 573 K [39–41]. Al–Zn phase diagram offers a

number of intermetallic compounds different in Al and Zn composition and metastable in structure. The solubility of Zn in (αAl) varies from 2,2 at.% at 383 K to 98,4 at.% at 550 K and maximum solubility of Al in Zn is 2,8 at.% at the eutectic temperature decreasing to 1,6 at.% at 550 K [39–41].

At the same time, the results show aluminium at EPMA recordings. Fig. 4, and some peaks other than those belonging to Zn and Al at GIXRD spectra obtained, Fig. 3 and Table 4. According to literature the most pronounced XRD peaks of Zn appear at $2\theta = 36,29°$, $38,99°$, $43,22°$, $70,07°$, $70,63°$, $82,09°$ [36, 37] and of Al at $2\theta = 38,47°$, $44,72°$, $65,10°$, $78,23°$, $82,43°$ [38]. The peaks for Al were not observed in our GIXRD spectra of zinc exposed to Al UPD, except for 2θ values close to $2\theta = 44,72$ which could be possibly attributed to Al (200) layer [35]. However, it was reported recently [33, 34] that Al peaks have not been observed in XRD spectra for Al–Zn alloys obtained by overpotential codeposition from ionic liquids containing Al and Zn at temperatures close to 383 K either.

Nevertheless, it appears that during aluminium underpotential deposition on zinc, under given conditions, rather thin surface alloys of metastable structures are formed. This is most probably due to self diffusions of Al and Zn in solid state and diffusion mobilities in solid solutions [43–45].

3.4. The growth of layers of alloys

Table 5 reports the maximum depths of the aluminium penetration into Zn substrate obtained by Auger spectroscopy. According to the theory expounded elsewere [17–19, 22] the thickness of each alloy layer, including ″buried″ ones, should increase with square-root of time, under solid state diffusion control. The charge of aluminium. $Q_{Al.(max)}$, dissolved from the Zn electrodes after Al underpotential deposition, at different temperatures and different times obtained from the linear sweep voltammograms are given in Table 2. These charges are time dependent and considerably higher than those corresponding to a close packed monolayer of aluminium, indicating the formation of an Al–Zn alloy in the region close to the interface.

Table 5. The depths (µm) of the formed aluminium layers on zinc samples after aluminium underpotential deposition for 2 hours and different temperatures obtained by Auger spectroscopy with sputtering rate 415 Å min^{-1}.

System	Temperature (K)		
	473	523	573
Al-Zn	0,01	0,03	0,08

Table 6. Calculated slopes (mC s$^{-1/2}$) for the curves in Figure 5.

System	Temperature (K)		
	473	523	573
Al-Zn	1,10	3,2	9,2

Fig. 5 shows plots of $Q_{Al.(max)}$ as a function of $\tau^{1/2}_d$ obtained from anodic parts of voltammograms at various temperatures. Linear relationships are observed with intercepts at $\tau_d = 0$. Corresponding calculated slope (mC s$^{-1/2}$) for the curves in Fig. 5 is given in Table 6. Under the assumption that the penetration depth (Δx) of the alloy into bulk substrate metal can be estimated from the equation:

$$\Delta x = \frac{M \, Q}{z \, F \, \rho} \qquad\qquad (1)$$

where: $M = 26{,}98$ g mol^{-1} and $\rho = 2{,}38$ g cm^{-3} are the atomic mass and the density of aluminium respectively, $z = 3$ is the charge involved per atom and Q is the charge involved in formation of alloy after deposition at E_d vs. Al for the time τ_d. Here Q is taken as the charge in excess of the value obtained from the extrapolation to τ_d i.e. $Q = Q_{Al.(max)} - Q_{Al.(max), \tau_d = 0}$. In fact this is thickness of an equivalent layer of pure aluminium, but it is difficult to make an easy correction for the density. The proportionality constant of the relationship between the thickness of each intermetallic layer and the square-root of time under solid state diffusion control, Table 6, depends on the difference in aluminium activity at the two phase boundaries, as well as on the mobility of aluminium.

4. CONCLUSIONS

The electrochemical techniques used showed underpotential deposition of aluminium from equimolar $AlCl_3$+NaCl melt on zinc substrate at temperatures ranging from 473 K to 573 K.

The UPD results in surface alloy formation by solid state diffusion of Al into the Zn substrate. Two, most probably metastable intermetallic compounds, were recorded, but their structure could not be identified.

The alloy layer thickness is dependant on the square-root of deposition time which was confirmed by „open circuit" anodic strriping.

The constant potential regions recorded during „open circuit" measurements correspond to the coexistence of pairs of intermetallic phases at the surface of zinc.

References

1. K. M. Gorbunova and Y. M. Polukarov, *Advances in Electrochemistry and Electrochemical Engineering,* Wiley, New York (1967).
2. A. R. Despić and V. D. Jović, *Modern Aspects of Electrochemistry,* Plenum Press, New York (1995).
3. G. R. Stafford and C. L. Hussey, *Advances in Electrochemical Science and Engineering,* Wiley-VCH Verlag GmbH, New York (2001).
4. C. L. Hussey, *Electroanalytical Chemistry in Molten Salts,* Marsel Dekker, New York (1996) 511.
5. G. Mamantov, C. L. Hussey and R. Marassi, *Techniques for characterization of electrodes and electrochemical processes,* John Wiley and Sons, New York (1991) 471.

6. V. D. Jović and J. N. Jovićević, *J. Appl. Electrochem.,* 19 (1989) 275.
7. M. Jafarian, F. Gobal, I. Danaee and M. G. Mahjani, *Electrochim. Acta*, 52 (2007) 5437.
8. W. Simka, D. Puszczyk and G. Nawrat, *Electrochim. Acta, 54* (2009) 5307.
9. C. Scordilis-Kelley, J. Fuller and R. T. Carlin, *J. Electrochem. Soc.*, 139 (1992) 694.
10. T. Tsuda, C. L. Hussey and G. R. Stafford, *J. Electrochem. Soc.,*152 (2005) C620.
11. P-Yu Chen and C. L. Hussey, *Electrochim. Acta*, 52 (2007) 1857.
12. D. MacFarlane, A. Abbott, *Electrodeposition from ionic liquids,* Wiley-VCH Verlag GmbH & Co, Weinheim (2008) 432.
13. D. M. Kolb, *Advances in Electrochemical Science and Engineering,* Wiley-VCH, Weinheim (2001).
14. E. Budevski, G. Staikov and W. J. Lorenc, *Electrochemical Phase Formation and Growth,*VCH, Weinheim (1996).
15. A. Bewick, J. N. Jovićević and B. Thomas, *Faraday Symposia of the Chem. Soc.,* 12 (1977) 24.
16. J. N. Jovićević and A. Bewick, *Facta Universitatis, Series Physics, Chemistry and Technology*, 3/2 (2005) 183.
17. H. Bort, K. Juttner, W. Lorenz and G. Staikov, *Electrochim. Acta*, 28 (1983) 993.
18. R.Vidu and S. Hara, *Surface Sci.,* 452 (2000) 229.
19. R.Vidu, N.Hirai and S.Hara, *Phys. Chem. Chem. Phys.*, 3 (2001) 3320.
20. B. S. Radović, *The growth and characterization of novel Al surface coatings prepared by underpotential deposition from low temperature melts,* PhD thesis, University of Strathclyde, Glasgow, UK (1992).
21. B. S. Radović, R. A. H. Edwards and J. N. Jovićević, *J. Electroanal. Chem.,* 428 (1997) 113.
22. B. S. Radović, R. A. H. Edwards, V. S. Cvetković and J. N. Jovićević, *Kovove mater.* 48, (2010) 55
23. B. S. Radović, V. S. Cvetković, R. A. H. Edwards and J. N. Jovićević, *Kovove mater.* 48, (2010) 159.
24. B. S. Radović, V. S. Cvetković, R. A. H. Edwards, J. N. Jovićević, *Int. J. Mat. Res.,* 102 (2011) 59.
25. Y. D. Yan, M. L. Zhang, Y. Hue, W. Han, D. X. Cao and L. Y. He, *J. Appl. Electrochem.,* 39 (2009) 455.
26. Q. Zhu, C. L. Hussey and G. R. Stafford, *J. Electrochem. Soc.,*148 (2001) C88.
27. J. J. Lee, I. T. Bae, D. A. Scherson, B. Miller and K. A. Wheeler, *J. Electrochem. Soc.*, 147 (2000) 562.
28. J. N. Jovićević, V. D. Jović and A. R. Despić, *Electrochim. Acta*, 29 (1984) 1625.
29. V. D. Jović and J. N. Jovićević, *Electrochim. Acta,* 30 (1985) 1455.
30. G. R. Stafford, O. E. Kongstein andG. M. Haarberg, *J. Electrochem. Soc.*, 15 (2006) C207.
31. L. Simanavičius, A. Stakenas and A. Šarkis, *Electrochim. Acta,* 42 (1997) 1581.
32. L. Simanavičius, A. Stakenas and A. Šarkis, *Electrochim. Acta,* 46 (2000) 499.
33. K. Takenaka, Y. Mizuta and T. Hirato, *Proc. III International Conference on Processing Materials for Properties (PMP-III),* December 7-10, Bangkok, Thailand, (2008) 213.
34. K. Takenaka, Y. Mizuta and T. Hirato, *ECS Transactions,* 29 (2009) 169.
35. P. Liddicoat, X. Liao, Y. Zhao, Y. Zhu, M. Murashkin, E. Lavernia, R. Valiev and S. Ringer, *Nature Communications,* doi:10.1038/ncomms1062
36. H. E. Swanson and E. Tatge, *Natl. Bur. Stand. (U.S.),* Circ. 539, 359 (1953) 1, Calculated from ICSD using POWD-12 (1997).
37. S. Ullah, A. Badshah, F. Ahmed, R. Raza, A. Ali Altaf, R. Hussain, *Int. J. Electrochim. Sci.*, 6 (2011) 3801.
38. M.E. Straumanis, *J. Appl. Phys.*, 20 (1949) 726.
39. Battelle Pacific Northwest National Laboratories, *MST Teachers Handbook,* U.S. Department of Energy, Pacific Northwest Laboratory, (2003).

40. MTDATA- Phase Diagram Software from the National Physical Laboratory, *Calculated Al-Zn phase diagram,* Updated 11 Novembar 2010.
41. *Binary Alloy Phase Diagrams,* Vol.1, Editor. T. D. Massalski, American Society for Metals, Metals Park, Ohio (1986).
42. W. Nernst, *Z. Phys. Chem.,* 4 (1889) 129.
43. O. Kubaschewski and E. L. Evans, *Metallurgical Thermochemistry,* Pergamon Press, New York (1958) 61.
44. L. S. Darken and R. W. Gurry, *Physical Chemistry of Metals,* McGraw-Hill, New York (1953) 675.
45. R. C. Salvarezza, D. V. Vasquezmoll, M. C. Giordano and A. J. Arvia, *J. Electroanal. Chem.,* 213 (1986) 301.